Topographically Induced Upwelling off Eastern Australia

PETER R. OKE

College of Oceanic and Atmospheric Sciences, Oregon State University, Corvallis, Oregon

JASON H. MIDDLETON

School of Mathematics, University of New South Wales, Sydney, Australia

(Manuscript received 7 October 1998, in final form 8 March 1999)

ABSTRACT

A high-resolution, numerical study of an idealized western boundary current flow over variable topography is presented, with application to the East Australian Current (EAC). The results indicate that alongshelf topographic variations off Australia's east coast cause the EAC to accelerate over the narrowing continental shelf near Cape Byron. This acceleration is sufficient to hinder the geostrophic adjustment in the bottom boundary layer (BBL), which would usually cause the EAC-driven BBL to shut down. Consequently, a region of persistent, high bottom stress was established off Cape Byron, which was responsible for driving an upwelling BBL. It is shown that the enhanced vertical mixing, associated with a low Richardson number flow beneath the EAC, reduced the local stratification. Consequently, the Burger number is decreased resulting in a long shutdown timescale of the BBL, which enables a nearshore thermal front to be established and maintained. Such fronts are commonly observed in the region. As a part of the analysis the term balances of the model equations are presented, comparing the dynamical balances at locations along the domain that exhibit varying degrees of topographic variability. The results indicate that the BBL dynamics were not purely geostrophic, further explaining why BBL shutdown was not prevailing. Moreover, it is shown that the formation of the thermal front was dependent on the magnitude of the EAC's southward transport, explaining why the occurrence of thermal fronts is greater during the spring and summer periods.

1. Introduction

The East Australian Current (EAC) is the western boundary current of the subtropical gyre of the south Pacific ocean. The EAC transports between 22 and 35 Sv (Sv $\equiv 10^6$ m^3 s^{-1}) southward along Australia's east coast (Ridgway and Godfrey 1997) with its strongest currents flowing adjacent to the continental shelf break (Cresswell 1994, 1999, manuscript in preparation) with currents up to 2 m s^{-1} (Church and Cresswell 1986). While the shelf currents associated with the EAC are typically weaker than the currents in the EAC's core, it is certain that, along with other factors such as local wind forcing (Gibbs et al. 1998), the EAC will have an effect on the nearshore zone (NSZ).

Thermal fronts have been observed in the EAC region on numerous occasions (Stanton 1976; Godfrey et al. 1980a; Cresswell et al. 1983; Tranter et al. 1986) with associated high levels of chlorophyl biomass on the continental shelf (Tranter et al. 1986). Several of these observations were made in the vicinity of Cape Byron during spring and summer, away from the EAC separation zone, which is located off Sugarloaf Point (Godfrey et al. 1980b) 500 km south of Cape Byron. The functional importance of thermal fronts, as indicators of high levels of biological activity, has long been recognized (Hynd 1969; Boucher et al. 1987; Hitchcock et al. 1993; Olsen et al. 1983; Franks and Walstad 1997). The aforementioned observations typically found that the temperature change across the front was 2°–3°C and that the front met the coast between Cape Byron and Tweed Heads. The sea surface temperature (SST) images displayed in Fig. 1, obtained from the *NOAA-11* satellite, show an example of a thermal front off Cape Byron, which occurred in October 1996. That fronts, similar to that in Fig. 1, are a regular seasonal feature prompts the following questions: How are the fronts formed? What factors effect their formation? Is their formation likely to result in the nutrient enrichment of the coastal waters? These questions are addressed through numerical experiments involving the configuration of a high-resolution regional ocean model off the central east coast of Australia. The experiments investigate the shelf response to a continuous, steady southward flow, characteristic of the EAC. The results show

Corresponding author address: Dr. Peter R. Oke, School of Mathematics, UNSW, Sydney, 2052 Australia.
E-mail: petero@maths.unsw.edu.au

© 2000 American Meteorological Society

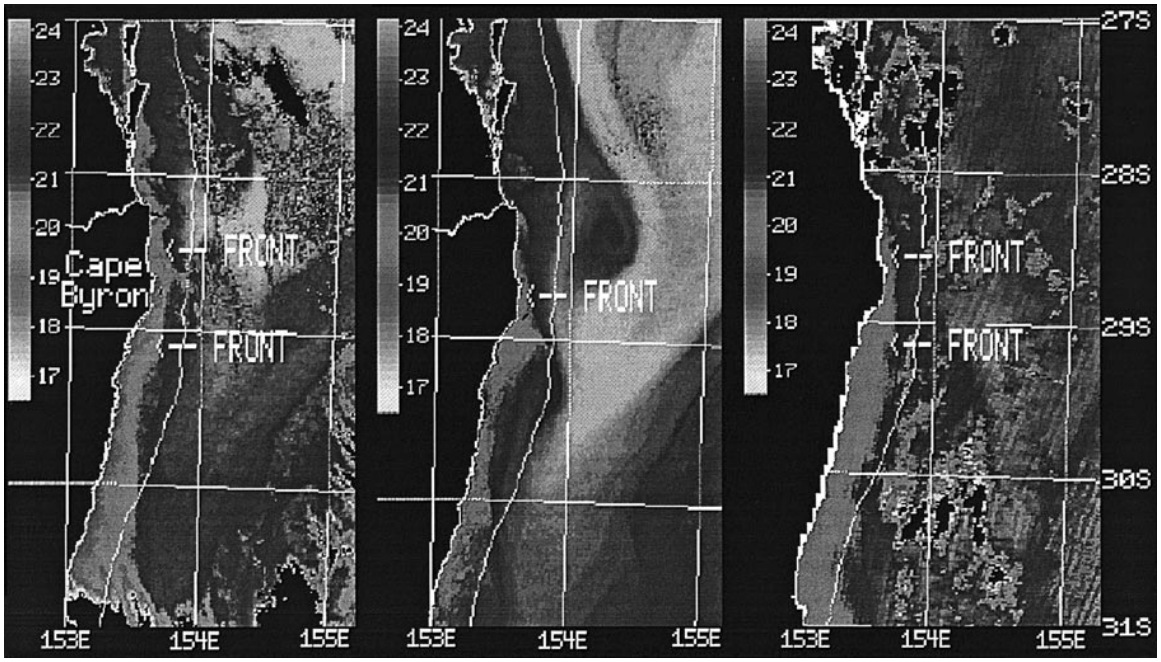

FIG. 1. SST fields of the study region for Oct 1996 showing an observed nearshore thermal front off Cape Byron. The 300-m isobath is contoured.

the formation of a nearshore thermal front, as a result of a persistent upwelling bottom boundary layer (BBL), driven by the alongshelf flow. The BBL shutdown process, which would be expected to inhibit such upwelling (MacCready and Rhines 1993), was not prevailing, and an analysis of the models internal dynamical balances was undertaken in order to identify the dominant dynamical processes.

Boundary layer theory of a stratified flow over a sloping shelf suggests that persistent current-driven upwelling is ineffective. The shutdown process is outlined below. If the bottom alongshelf velocity v_B is nonzero, then an alongshelf bottom stress τ_b^y is induced such that

$$\tau_b^y = C_D v \sqrt{u_B^2 + v_B},$$

where C_D is the bottom drag coefficient. In western boundary current regions, such a stress will drive an upwelling BBL as depicted in Fig. 2. This upwelling

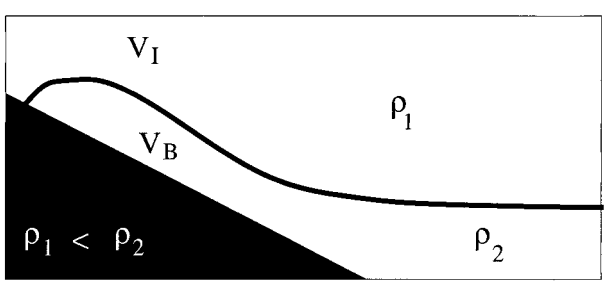

FIG. 2. Schematic depicting the upwelling of a stratified flow over a sloping bottom, where v_I and v_B denote the interior and bottom velocity (directed out of the page), respectively.

will then result in a horizontal density gradient $\partial\rho/\partial x$ between the upwelled BBL water (ρ_2) and the interior water (ρ_1) where $\rho_1 < \rho_2$. Under a geostrophic assumption the thermal wind relation

$$\frac{\partial v}{\partial z} = -\frac{g}{\rho_0}\frac{\partial \rho}{\partial x} \tag{1}$$

acts to reduce the alongshelf bottom velocity v_B to zero by increasing the vertical velocity gradient $\partial v/\partial z$. Consequently, the alongshelf bottom stress formulated above also reduces to zero. In the absence of a bottom stress, a frictional BBL cannot be maintained and, consequently, shuts down. Equation (1) is derived by assuming that the cross-shelf momentum balance of the flow is geostrophic. Results from this study indicate that such an assumption off Cape Byron, where the alongshelf topography varies considerably, is inadequate, with the vertical diffusion term playing a significant role. It is shown through an analysis of the internal dynamical balances that the EAC accelerates, in a Lagrangian sense, in the vicinity of Cape Byron in response to topographic constraints. As a result of this acceleration the Richardson number Ri, defined as

$$\mathrm{Ri} = \frac{N^2}{u_z^2 + v_z^2}, \tag{2}$$

where N^2 is the bouyancy frequency, is reduced below the critical value of 0.25, resulting in increased values of the vertical, turbulent eddy viscosity K_m (Mellor and Yamada 1982), which results in a persistent Ekman-like balance near the bottom over the shelf. The strong ver-

tical mixing in the BBL causes the buoyancy frequency to decrease, which in turn decreases the local Burger number S, defined as

$$S = \frac{N^2\alpha}{f^2}, \tag{3}$$

where α is the bottom slope and f is the Coriolis parameter. Boundary layer theory states that a small Burger number flow corresponds to an increased shutdown time τ_S, where

$$\tau_S \approx \frac{1}{Sf} \tag{4}$$

if the turbulent Prandlt number is assumed to be unity (Garret et al. 1993). The increased shutdown time explains why the BBL flow was so persistent, enabling a nearshore thermal front to become established. The analysis of the term balance for the conservation equation for temperature indicated that, although an upwelling BBL was persistent, the rate of upwelling of isotherms decreased with time. It appears as if an ''upwelling limit'' is approached, where the slope of the isotherms (or isopycnals) match that of the bottom slope, thereby allowing for along-isopycnal transport to be maintained, uninhibited by the opposing forces of bouyancy.

The correlation of upwellings to EAC encroachments onto the continental shelf was first identified by Rochford (1972) who suggested that, ''when the core of a strong south-flowing current nears the continental slope, temperatures of mid-depth waters over the slope are much reduced'' near Cape Byron. Furthermore, Rochford's (1972) observations indicated that the cold, upwelled waters were typically upwelled to the surface between Evans Head and Cape Byron. Similarly, Rochford (1975) suggested that upwellings off Laurieton, on the New South Wales (NSW) central coast, were the result of the EAC flow intruding onto the continental shelf, explaining events that were seemingly unrelated to the local winds. These suggestions by Rochford are more fully explored by Oke and Middleton (2000), where the separation of the EAC from the coast was shown to play a crucial role. The observations made by Rochford (1975) off Evans Head during periods of upwelling showed that the isotherm slope was very close to that of the bottom topography, consistent with the results mentioned above.

The numerical experiments presented here involve a detailed comparison of two model configurations, a local domain model (LDM) and an extended domain model (EDM). Since regional ocean modeling necessitates the use of open boundary conditions of some description, then the boundary values, and their effect on the model circulation remain uncertain (Mahadevan et al. 1996). Consequently, it is argued that, if the same results are obtained for a small regional model and a larger regional model where the boundaries are well away from the area of interest, then the results are robust and the model circulation is deemed to be relatively insensitive to the proximity of the lateral boundaries. The results from both models are shown to agree; however it is clear that there is an advantage with the larger EDM since the imposed flow had sufficient time to adjust to the local topography before encountering the complex, variable topography. Additional sensitivity experiments were also performed with the EDM in order to investigate the dependence of the model dynamics on the transport magnitude, stratification, and grid resolution, and it is shown that the persistent BBL flow is dependent on the transport magnitude, which explains why more fronts are encountered off Cape Byron in spring and summer when the EAC's transport is typically stronger (Ridgway and Godfrey 1997).

This paper is organized with a description of the model configurations and the boundary conditions presented in section 2. The results are presented in section 3, which includes an analysis of a sensitivity study, and an analysis of the internal dynamical balances of the model equations is in section 4. A discussion of the results is presented in section 5 followed by the conclusions in section 6.

2. Model configurations

The model used in this study is the Princeton Ocean Model (POM). Briefly, the POM is a hydrostatic, free-surface, sigma-coordinate, primitive equation model, with an embedded turbulence submodel. For an in-depth description of the model equations and the numerical techniques, the reader is referred to Blumberg and Mellor (1987). Details of the two model configurations used are presented below.

a. Local domain model

The LDM extends between latitudes 29°38′S and 27°23′S covering an alongshelf distance of 250 km, extending out to 125 km offshore (Fig. 3). A rectangular grid was used consisting of 81 × 111 points, with cross-shelf grid spacings of 1 km over the shelf and slope increasing to 4 km near the seaward boundary. Similarly, the alongshelf grid spacings were 2 km over most of the interior, increasing to 4 km over a distance of 25 km near each of the alongshelf boundaries. The vertical grid consisted of 31 vertical levels varying linearly over middepths and logarithmically over upper and near-bottom depths. The model bathymetry was extracted from the ETOPO5 dataset (NOAA 1988) with a minimum depth of 20 m. The maximum depth was set to 1000 m in order to reduce the constraint on the time steps, which were 4.25 and 135 s for the barotropic and baroclinic modes, respectively. In order to interpolate the bathymetry onto the model grid the bathymetry locations were first converted to the Australian Map Grid. The bathymetry was then rotated in an anticlockwise direction

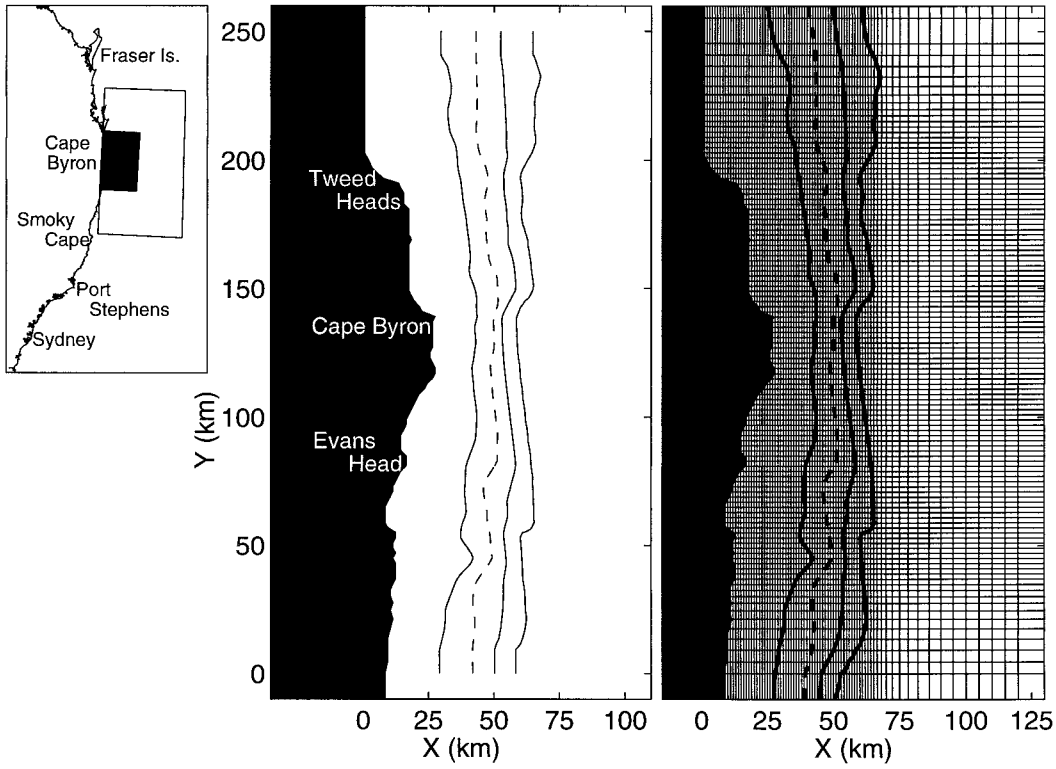

FIG. 3. Study location (left) showing the extent of the local domain (filled) and the extended domain (outlined); model bathymetry (middle) showing the 100, 200 (dashed), 500, and 1000 m isobaths; the model grid (right) for the local domain model.

by 10° in order to align the isobaths with the alongshelf direction of the grid, and finally the bathymetry was linearly interpolated onto the model grid. The bathymetry was then weakly smoothed in order to regulate the maximum local slope parameter r, defined by

$$r = \frac{\Delta x, yH}{\overline{H}},$$

which represents the ratio of the change in depth Δx, yH, to the average depth $\overline{H}$ over each grid cell (Mellor et al. 1994). As a general rule, the maximum value of r should be less than 0.2 in order to sufficiently reduce the pressure gradient errors associated with the sigma coordinates (Beckmann and Haidvogel 1993). Within this configuration the maximum slope parameter was 0.17, satisfying this criterion. The Coriolis parameter was rotated and interpolated in an analogous fashion to the bathymetry so that no f-plane or β-plane approximations were necessary in the LDM.

The upper 200 m of the temperature field was initialized with the mean temperature profile extracted from conductivity–temperature–depth (CTD) data collected near Cape Byron during October 1996 (Oke and Middleton 2000, manuscript in preparation, hereafter OM). The spatial details of the CTD measurements were not representative of the time averaged field due to the presence of a highly dynamic internal tide on the shelf at the time of sampling, and as such were not included in the model initialization. The temperature below 200-m depth corresponds to the spring, climatological values for the region as specified by Levitus (1982). The initial temperature field was defined with preconditioned isotherms tilting upwards towards the coast, a feature typical of a cross-shelf temperature section for the EAC region (Fig. 4). The temperature field was initially homogeneous in the alongshelf direction. For simplicity the salinity was set to a constant value of 35 psu throughout the model domain.

The initial currents were defined by an idealized Gaussian jet of width 80 km and a maximum speed of 0.8 m s^{-1} at the surface. The jet was centred over the 300-m isobath, adjacent to the shelf break, and the baroclinic structure of the current was estimated from the thermal wind relation. The resulting southward transport was 14 Sv, which is much less than the EAC's seasonal average of 27 Sv (Ridgway and Godfrey 1997). However, given the unrealistic maximum depth of 1000 m, this transport was deemed representative of a baroclinic EAC flow. The initial Burger number of the flow over the shelf was greater than 0.29, which corresponds to a BBL shutdown time of 2 days from Eq. (4).

The boundary conditions implemented at the southern boundary included zero gradient and upstream advection conditions for the baroclinic variables (Blumberg

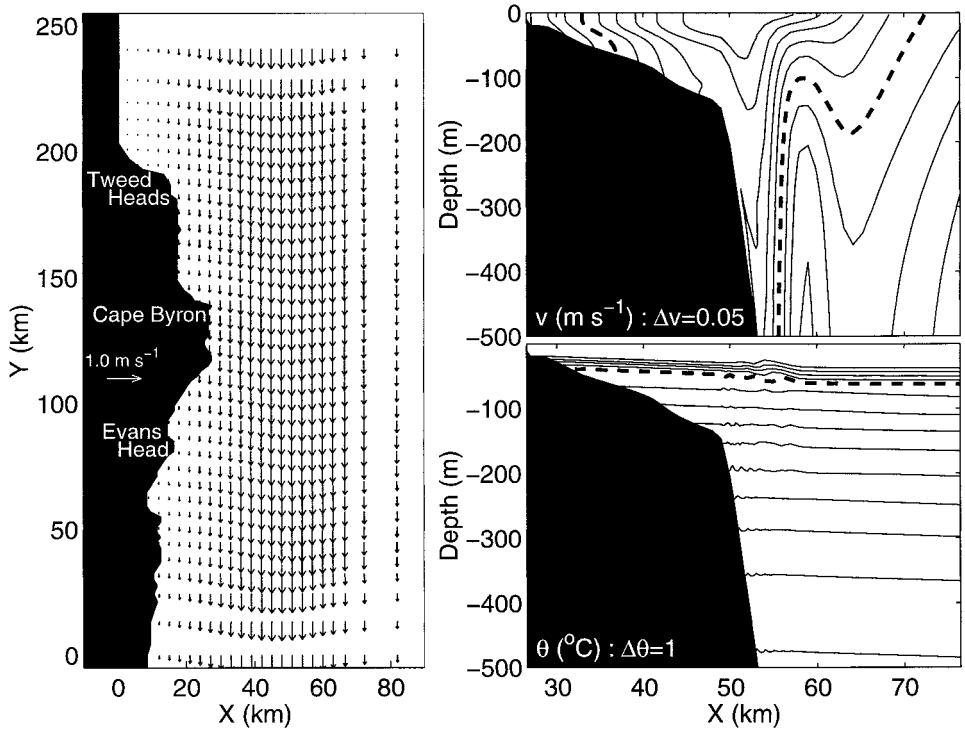

FIG. 4. Initial surface velocity field (left, showing every third vector), alongshelf velocity structure (top right) and temperature section (bottom right) showing the 0.5 m s^{-1} and 20°C (bold dashed) contours respectively off Cape Byron ($Y = 135$ km).

and Mellor 1983) and modified radiation conditions for the barotropic variables (Flather 1976; Blumberg and Kantha 1985; Palma and Matano 1998). These conditions allow the time averaged barotropic flow at the boundary to be imposed, or relaxed over a specified timescale (2 days). Consequently, the boundary values were ''controlled,'' while disturbances generated within the domain were allowed to propagate out with minimal reflection. All variables were prescribed at the northern boundary throughout the simulations. The seaward boundary ($X = 125$ km) was masked by a vertical wall, a feature which is unrealistic, but not critical for the present study, due to the absence of wind forcing.

b. Extended domain model

For the EDM the bathymetry from the boundaries of the LDM were extended an additional 150 km offshore and in both alongshelf directions. The alongshelf grid spacings were increased to 10 km in the extended region, leaving the part of the domain common to both the LDM and the EDM unchanged. Similarly, the Coriolis parameter was uniformly set to the LDM's boundary values over the extended region. The resulting EDM consisted of 96 × 141 horizontal grid points and 31 vertical levels.

The rationale behind comparing the LDM and the EDM simulations was to assess the sensitivity of the model to the proximity of the lateral boundary forcing. One characteristic of the open boundary conditions implemented into the configuration is that the amplitude and structure of the volume transport was able to be imposed. The advantage of this is that a volume conserving configuration could be obtained; however it assumes that the time averaged barotropic boundary values were known a priori. It is therefore unclear to what extent the model circulation will depend on these boundary values. In the LDM the boundaries were very close to the area of interest, namely Cape Byron, however the EDM had the boundaries 150 km farther away in all directions. Consequently, it is proposed that if the LDM and the EDM's results are in agreement, then the model circulation is robust, and hence valid for the idealized scenario outlined in section 1.

3. Results

The simulations presented below were run prognostically for 15 days. All variables presented hereafter represent averages over an inertial period. For the results below, fields from both the LDM and the EDM are shown for comparison.

a. Model spinup

As a first assessment of the model's performance the temporal evolution of the percentage change of the area

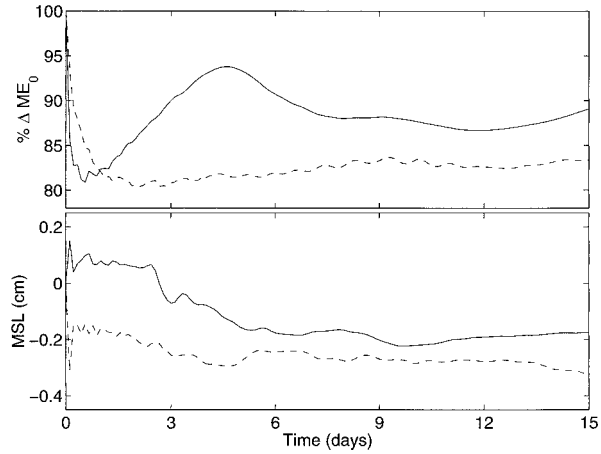

FIG. 5. Area averaged % ΔME_0 (top) and MSL (bottom) for the local domain (solid) and extended domain model (dashed).

averaged mechanical energy from the initial state % ΔME_0 was calculated, such that

$$\% \ \Delta ME_0 = \frac{1}{A_T}\left(\int_A \overline{\rho} g \eta^2 + 0.5\overline{\rho} H(\overline{u}^2 + \overline{v}^2)\, dA\right) \div ME_0 \times 100,$$

where ME_0 is the initial mechanical energy, A_T is the area of the domain, $\overline{\rho}$ is the depth averaged density, η is the elevation, H is the water depth, and $\overline{u}$ and $\overline{v}$ are the cross-shelf and alongshelf depth averaged velocities respectively (Palma and Matano 1997). As an additional measure of the model's performance, the mean sea level (MSL) was evaluated, where

$$MSL = \frac{1}{A_T}\int_A \eta \, dA.$$

These properties of the simulations are presented in Fig. 5, indicating that, after an initial adjustment, the mechanical energy reached a state of ''zonal equilibrium'' after approximately 7 days in the LDM and 1 day in the EDM. Furthermore, the MSL similarly indicated that after an initial adjustment the volume of both models were conserved. These observations indicate that the boundary conditions were satisfactory in terms of maintaining a constant energy and volume flux through the model domain. Having satisfied these important criteria, we shall now turn to a qualitative comparison between the LDM and the EDM simulations.

b. Simulated baroclinic fields

Given that the model initializations of both configurations were equivalent, perturbations in temperature and alongshelf velocity, θ' and v', are presented such that

$$\theta'_n = {}_n\theta_n - \theta_0 \quad \text{and} \quad v' = v_n - v_0,$$

where the subscripts denote simulation days. As we shall see, consideration of these variables give insight into the internal adjustments made within the model simulations.

The area of interest for this study was the continental shelf off Cape Byron, situated in the center of the model domain. The simulated baroclinic fields on day 15 are presented in Fig. 6. The alongshelf velocity perturbation indicates that the velocity decreased over near-bottom depths in response to bottom friction, and conversely increased slightly over mid and upper depths in order to conserve the alongshelf transport. The cross-shelf velocity fields show a shoreward BBL flow in the bottom 15 m of water over the continental shelf with currents in excess of 0.05 m s^{-1}. This BBL transport extends across the entire continental shelf and past the shelf break.

As a consequence of this shoreward BBL flow isotherms were advected toward the coast resulting in a decrease in temperature over the shelf and NSZ. This is clearly evident in the temperature perturbation fields, showing a decrease of the temperature in the NSZ by greater than 7°C.

The results from both the LDM and the EDM were in good agreement, although the LDM shows the temperature decrease over a greater area on the shelf. The above comparison indicates that the baroclinic perturbations from the initial state were similar for both model configurations.

c. Bottom stress

The fields of bottom stress, presented in Fig. 7, indicate that there was high bottom stress between Tweed Heads (Y = 188 km) and Evans Head (Y = 80 km). The overall pattern of the bottom stress fields was similar for both the LDM and the EDM; however the magnitude of the stress was greater in the LDM off both Tweed Heads and Evans Head. There was also a region of high bottom stress to the north of Tweed Heads near the northern boundary of the LDM. This feature is evidence of the model circulations internal adjustment due to the idealized structure of the imposed lateral forcing. By moving the northern boundary farther north in the EDM and allowing the model circulation to adjust before encountering the varying topography, this effect was significantly reduced.

The region of highest bottom stress in both models was evident adjacent to Cape Byron, extending from the coast to beyond the 200-m isobath. This feature explains the persistent shoreward BBL flow presented above as EAC-driven uplifting caused by the currents frictional interaction with the local topography. There is also an isolated region of high bottom stress off Evans Head. A dynamical explanation of this feature is postponed to section 5. The similarities between the bottom stress fields in the LDM and the EDM give confidence in the robustness of the model results. The nearshore effects

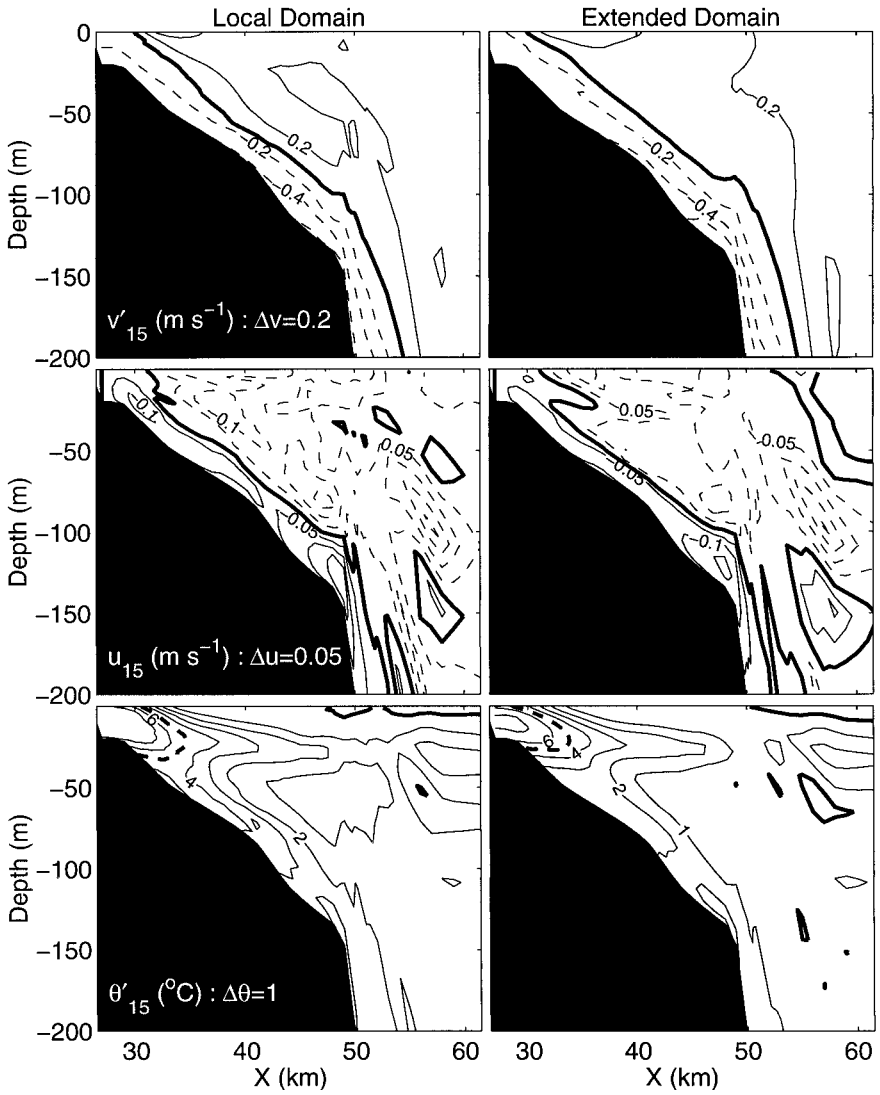

FIG. 6. Cross section adjacent to Cape Byron (Y = 135 km) of the v'_{15}, u and $-\theta'_{15}$ showing the zero velocity (bold solid) and −5°C (bold dashed) contours.

of this region of high bottom stress can be seen by considering the near-surface temperature field.

d. Near-surface temperature

The extent of the EAC uplifting can be seen in the near-surface temperature perturbation field at day 15 (Fig. 8). These fields indicate that the temperature near Cape Byron dropped by 8°C in the LDM and 7°Ci n the EDM. More uplifting was simulated in the LDM, arguably due to the closeness of the lateral boundaries; however qualitatively, the results are very similar. The region of greatest temperature decrease in the NSZ correlates well with the alongshelf locations of the high bottom stress discussed above.

The temperature decrease represents the formation of a nearshore thermal front, concentrated near Cape Byron, extending toward Tweed Heads. This description is similar to the nearshore thermal front observed by OMb and also by Godfrey et al. (1980a) in the same region.

e. Sensitivity experiments

As well as the comparison between the LDM and the EDM, additional numerical simulations have been performed in order to assess the dependence of the model circulation on the transport magnitude, stratification and grid resolution. A list of these experiments, and a brief description of each is presented in Table 1. The resulting baroclinic cross-sections of alongshelf velocity, across-shelf velocity and temperature fields off Cape Byron (Y

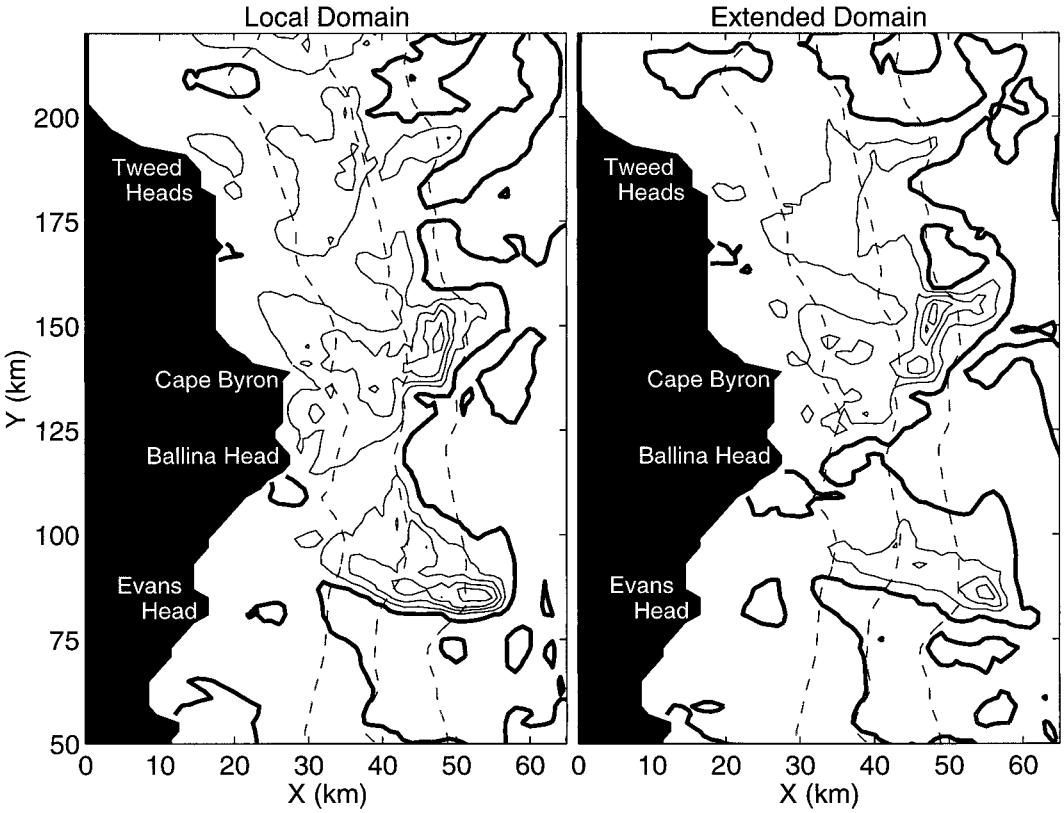

FIG. 7. Bottom stress at day 15 with contour intervals of 1×10^{-4} m^2 s^{-2} showing the zero contour (bold solid) and the 50, 100, and 200-m isobaths (dashed).

= 135 km) on day 15 for various simulations is shown in Fig. 9. It is found that a persistent shoreward BBL was present in all experiments, although there was a clear dependence on the magnitude of the transport, with a weaker (stronger) BBL flow generated above the shelf break by a reduced (increased) transport. Furthermore, for experiment 5, which had a weak southward transport, the BBL flow was not maintained from the shelf break to the coast, unlike all other experiments. This dependence explains the seasonal variation of the occurrance of nearshore fronts off Cape Byron. This appears to be a result of the fact that the southward currents in the NSZ were weaker and, more significantly, had less vertical shear. The reduced vertical shear effectively increased the Richardson number, decreasing the magnitude of the vertical diffusion term in the momentum equations, which is important for the BBL flow to be maintained as we shall see in section 4. Results from experiments 7 and 8 with increased and decreased horizontal resolutions producing very similar results to the LDM and EDM results presented above.

Possibly the most significant features of the cross-shelf sections presented in Fig. 9 is that the slope of the isotherms over the shelf is very close to that of the bottom slope. This synoptic feature is consistent with the observations made by Rochford (1972) who observed that upwelling near Cape Byron, that was seemingly unrelated to local wind forcing, involved isotherms originating at the depth of the shelf break being transported into the NSZ. When the slope of the isotherms (or isopycnals, given that salinity is constant) match the bottom slope, along-isopycnal mixing is possible, whereby water originating from within the depth of the shelf break and beyond can be upwelled to the surface, without being inhibited by the opposing effects of bouyancy. This implies that nutrient enrichment of the NSZ will be very efficient under these conditions. The isotherms are close to, but not quite parallel to, the bottom slope on day 15; however, an assessment of the temporal behavior of the temperature decrease can be determined by considering a time series of the temperature in the NSZ and adjacent to the shelf break (Fig. 10). These time series show that the upwelling of isotherms continued well after the models had spun up; however an ''upwelling limit'' seems to be inevitable. Based on the arguments presented above, this upwelling limit represents the situation where the isotherm slope matches that of the bottom slope, which implies that current-driven upwelling will always be limited to upwelling water originating no deeper than the shelf break. The reason for this is that beyond the shelf break the Burger number dramatically increases, so the shutdown timescale decreases.

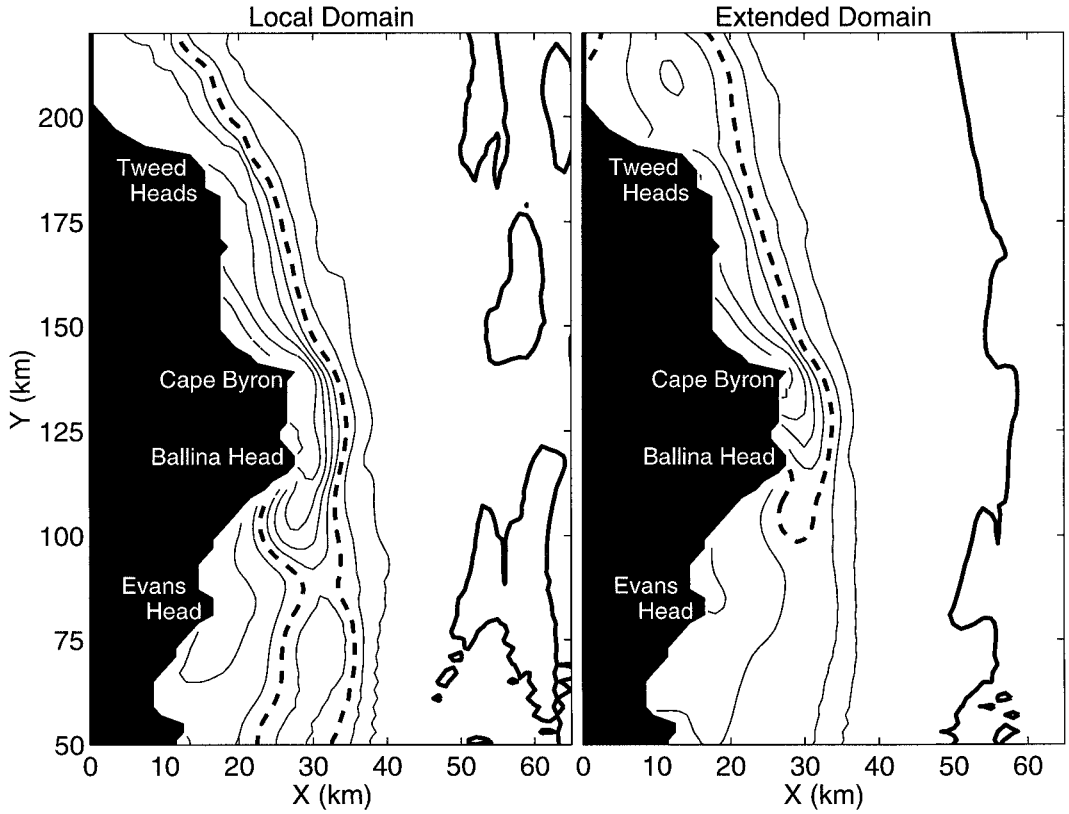

FIG. 8. Temperature perturbation at day 15 with contour intervals of 1°C showing the 3°C (bold dashed) contour.

4. Internal dynamical balances

The ''terms'' in the momentum equations and the conservation equation for temperature were averaged over an inertial period and extracted from the EDM at day 15 (experiment 2). The terms were then averaged over seven consecutive grid cells in the alongshelf direction, in order to ensure that the dynamical balances are valid for the ''zones'' of interest. Three zones have been selected for analysis, and their locations are presented in Fig. 11. The first is north of Tweed Heads (Y = 208 km), which is located at the northern extent of the variable topography region of the model. This zone was chosen to act as the control for this analysis in order to determine the effects of the variable topography located farther downstream. The second zone selected is adjacent to Cape Byron (Y = 135 km), the site of the EAC-driven BBL upwelling presented in section 3. The third zone is off Evans Head (Y = 76 km), which was again a site of high bottom stress over the mid to outer shelf.

TABLE 1. Summary of the numerical experiments for which simulations were performed, indicating the model grid, buoyancy frequency N^2, southward transport (T), and grid resolution of the circulation.

Exp	Description
1	LDM, $N^2 = N_0^2$, T = 14 Sv
2	EDM, $N^2 = N_0^2$, T = 14 Sv
3	EDM, $N^2 = 2N_0^2$, T = 14 Sv
4	EDM, $N^2 = 0.5N_0^2$, T = 14 Sv
5	EDM, $N^2 = N_0^2$, T = 7S v
6	EDM, $N^2 = N_0^2$, T = 21 Sv
7	EDM, $N^2 = N_0^2$, T = 14 Sv, $\Delta x = 2\Delta x_0$
8	EDM, $N^2 = N_0^2$, T = 14 Sv, $\Delta x = ½\Delta x_0$

We have considered the term balances in sigma coordinates at constant sigma levels near the surface ($\sigma = -0.043$), at mid depths ($\sigma = -0.478$) and at near-bottom depths ($\sigma = -0.913$), after Allen et al. (1995), as indicated in Fig. 11. Based on the results presented above, the near-bottom level represents the dynamics of the BBL throughout the simulation, while the mid and near-surface depths represent the interior EAC flow.

a. Momentum balance

The terms in the alongshelf and cross-shelf momentum balances include the tendency, advection, rotation, pressure gradient, vertical diffusion, and the horizontal diffusion terms. The generic name and short-hand notation are presented below. The short-hand notation is not intended to represent each term in a strict mathe-

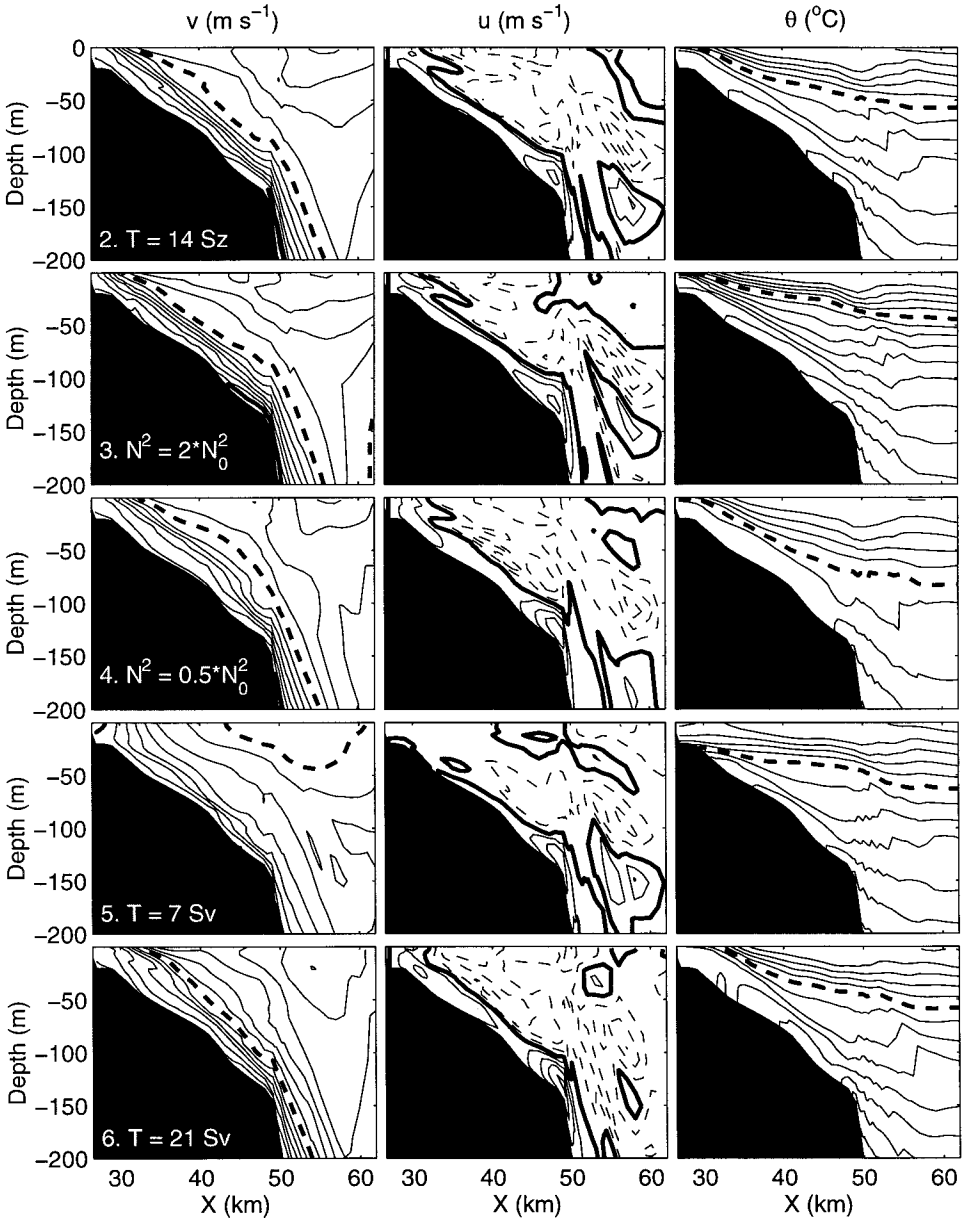

FIG. 9. Cross-sections of alongshelf velocity, cross-shelf velocity and temperature (left to right) off Cape Byron (Y = 135 km) for various sensitivity experiments described in Table 1.

matical sense; rather, it is employed as a matter of convenience. For a fuller presentation of the model equations, the reader is refered to Blumberg and Mellor (1987). The terms balance for the alongshelf and cross-shelf momentum equations are represented by

$$\text{tendency} + \text{advection} + \text{rotation} - \text{pressure gradient}$$
$$- \text{vertical diffusion} - \text{horizontal diffusion} = 0$$
$$v_t + \mathbf{v} \cdot \nabla v + fu - P - (K_m v_z)_z - A_m v_{xx} = 0,$$
$$u_t + \mathbf{v} \cdot \nabla u - fv - P - (K_m u_z)_z - A_m u_{xx} = 0,$$

where $\mathbf{v}$ is the velocity vector with components (u, v, w), corresponding to the cross-shelf, alongshelf and vertical directions (x, y, σ). The operator $\nabla = (\partial/\partial x, \partial/\partial y, \partial/\partial z)$; t is time, f is the Coriolis parameter, and P is pressure. Here K_m is the turbulent eddy viscosity, determined by the flow-dependent Mellor–Yamada 2.5 closure scheme (Mellor and Yamada 1982), and A_m is the flow-dependent horizontal eddy viscosity, determined by the formulation of Smagorinsky (1963). All of the terms in the momentum equations were multiplied by a scaling factor of $D^{-1}\,\Delta t \times 10^3$, where D is the height of the water

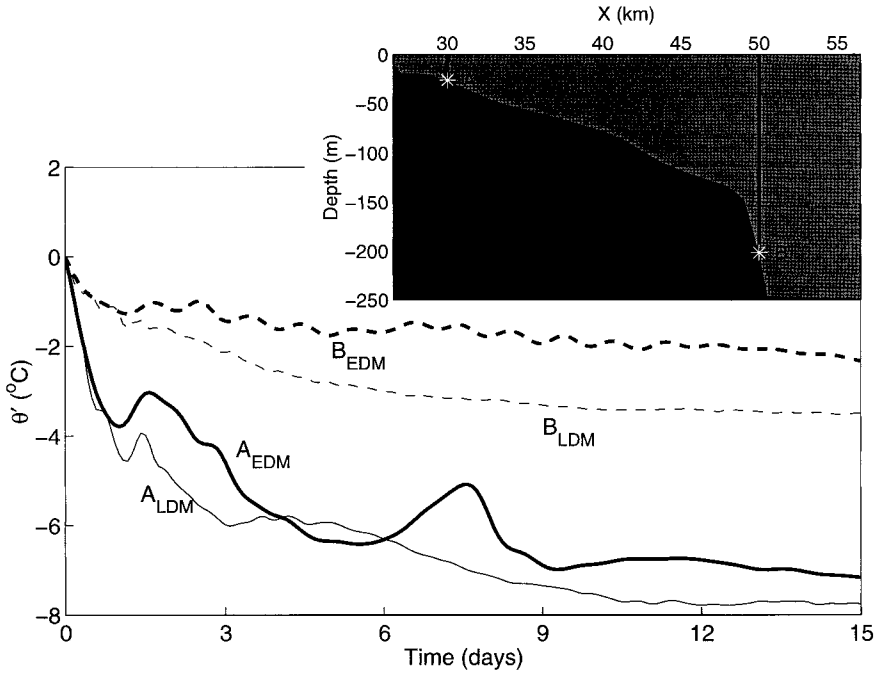

FIG. 10. Time series of hourly temperature perturbation from the NSZ (a) and adjacent to the shelf break (b) as indicated by an asterisk off Cape Byron.

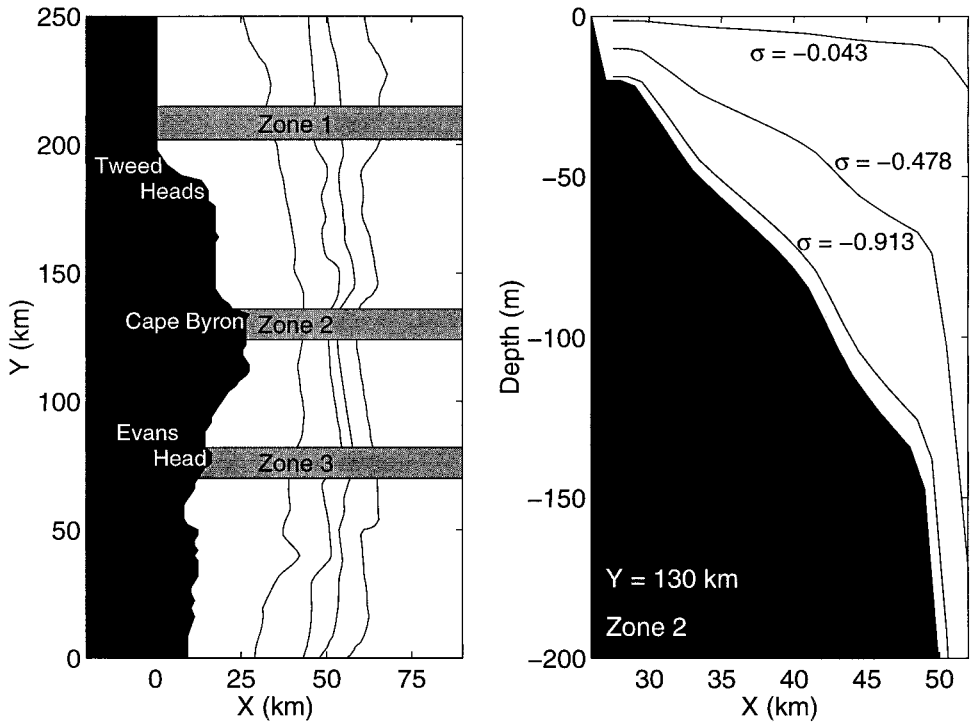

FIG. 11. Alongshelf locations of zones for which the alongshelf momentum balance is presented (left) and the depths of the sigma levels representing the near-surface, middepth, and near-bottom levels.

column and Δt is the baroclinic time step, giving them units of (m s^{-1}) $\times$ 10^3.

b. Conservation equation for temperature

The terms balance in the conservation equation for temperature include the tendency, advection, vertical diffusion and the horizontal diffusion terms. The generic name and short-hand notation are given by

$$\text{tendency} + \text{advection} - \text{vertical diffusion} - \text{horizontal diffusion} = 0$$

$$\theta_t + {}_h\mathbf{v} \cdot \nabla\theta - (K\,\theta_z)_z - A_h\theta_{xx} = 0,$$

where θ is the temperature, K_h is the vertical diffusivity for heat, and A_h is the horizontal diffusivity for heat. In the POM, K_h is determined by the turbulence submodel of Mellor and Yamada (1982) and A_h is taken to be proportional to the horizontal viscosity A_m, which was determined by the Smagorinsky scheme (Smagorinsky 1963). The turbulent Prandlt number, which relates the values of A_h and A_m, was set to unity for the simulations considered. Increasing the Prandlt number simply increases the horizontal smoothing of the temperature field. The horizontal diffusion term is meant to model the subgrid scale processes; however in practice it is employed to damp small-scale computational noise (Blumberg and Mellor 1987). All of the terms in the conservation equation presented were multiplied by a scaling factor of $D^{-1}\,\Delta t \times 10^3$ giving them units of °C $\times$ 10^3.

The resulting terms balance for the alongshelf and cross-shelf momentum equations and for the conservation equation for temperature, for each zone on day 15, are presented in Figs. 12 and 13, and 14, respectively. The near bottom balances are presented separately from the mid depth and near-surface balances since they are of particular interest with regard to the upwelling mechanism presented in section 3.

c. Near-bottom depths

The alongshelf momentum balance to the north of Tweed Heads, in zone 1, indicates that near the bottom, the dominant balance was between P_y and fu over the mid and outer shelf, representing a geostrophic balance. Vertical diffusion, $(K_m v_z)_z$, also becomes important in the NSZ, being balanced by P_y and fu, representing an Ekman-like balance. The cross-shelf momentum balance was almost purely geostrophic in this zone. The conservation balance in zone 1 indicates a balance between small, negative θ_t and positive $\mathbf{v} \cdot \nabla\theta$, which represents a weak upwelling of isotherms, representing the initial response of the southward flow to variable topography.

In the region adjacent to Cape Byron, represented here by zone 2, there was a persistent upwelling BBL flow throughout the simulation resulting in the formation of the nearshore thermal front. The near-bottom dynamical balance at zone 2 was very different to zone 1, indicating that $(K_m v_z)_z$ was the dominant term between the coast and the 200-m isobath. Negative $(K_m v_z)_z$ was balanced by positive P_y and fu. The increased magnitude of $(K_m v_z)_z$ indicates that there was enhanced vertical mixing above the bottom due to frictional effects from beneath the EAC that were acting to retard the bottom currents. Furthermore, the positive fu term indicates that an upwelling BBL flow was present, and that both fu and P_y were positive indicates that the flow was not in geostrophic balance. Rather, these dynamics are more consistent with a three dimensional, linear Ekman balance. The balance is not totally linear, since $\mathbf{v} \cdot \nabla v$ was also of secondary importance. The near bottom balance of the cross-shelf momentum equations was in quasigeostrophic balance with $(K_m u_z)_z$ also being important. The significance of the near-bottom flow being out of geostrophic balance has implications for the validity of the MacCready and Rhines (1993) BBL shutdown theory in regions of varying topography. This suggestion will be further investigated below, with a reconstruction of the terms in the thermal wind relation from the modeled fields.

The conservation balance indicates that negative $(K_h\theta_z)_z$ was balanced by positive $\mathbf{v} \cdot \nabla\theta$. Over the shelf break and in the NSZ θ_t was small and negative, indicating a weak upwelling; however over the midshelf region θ_t was small and positive. The implications of these features will be fully discussed in section 5. Additionally, the NSZ exhibited a high degree of complexity, in agreement with the inferences of OM.

Zone 3 was located to the south of Cape Byron, off Evans Head. The alongshelf momentum balance seaward of the 100-m isobath was similar to zone 2, with $\mathbf{v} \cdot \nabla v$ of increasing importance. The near-bottom frictional influence was isolated to the shelf-break region, which correlates well with the distribution of bottom stress presented in section 3. In the NSZ a more geostrophic balance was evident, with a dominant balance between positive fu and negative P_y, although $(K_m v_z)_z$ was also important adjacent to the coast. The advection term $\mathbf{v} \cdot \nabla v$, became increasingly less important towards the coast, consistent with the conceptual views of the EAC flow as a strong, narrow jet over the shelf break.

It is clear that across the entire shelf at Cape Byron the BBL dynamics were not purely geostrophic as indicated by the fact that P_y and fu had the same signs in the alongshelf momentum balance and that $(K_m u_z)_z$ was significant in the cross-shelf momentum balance. The magnitude of fu in zones 2 and 3 was greater than zone 1 indicating that the BBL flow was stronger at these locations.

d. Mid and near-surface depths

Over mid and near-surface depths across most of the shelf the dominant terms in the alongshelf momentum

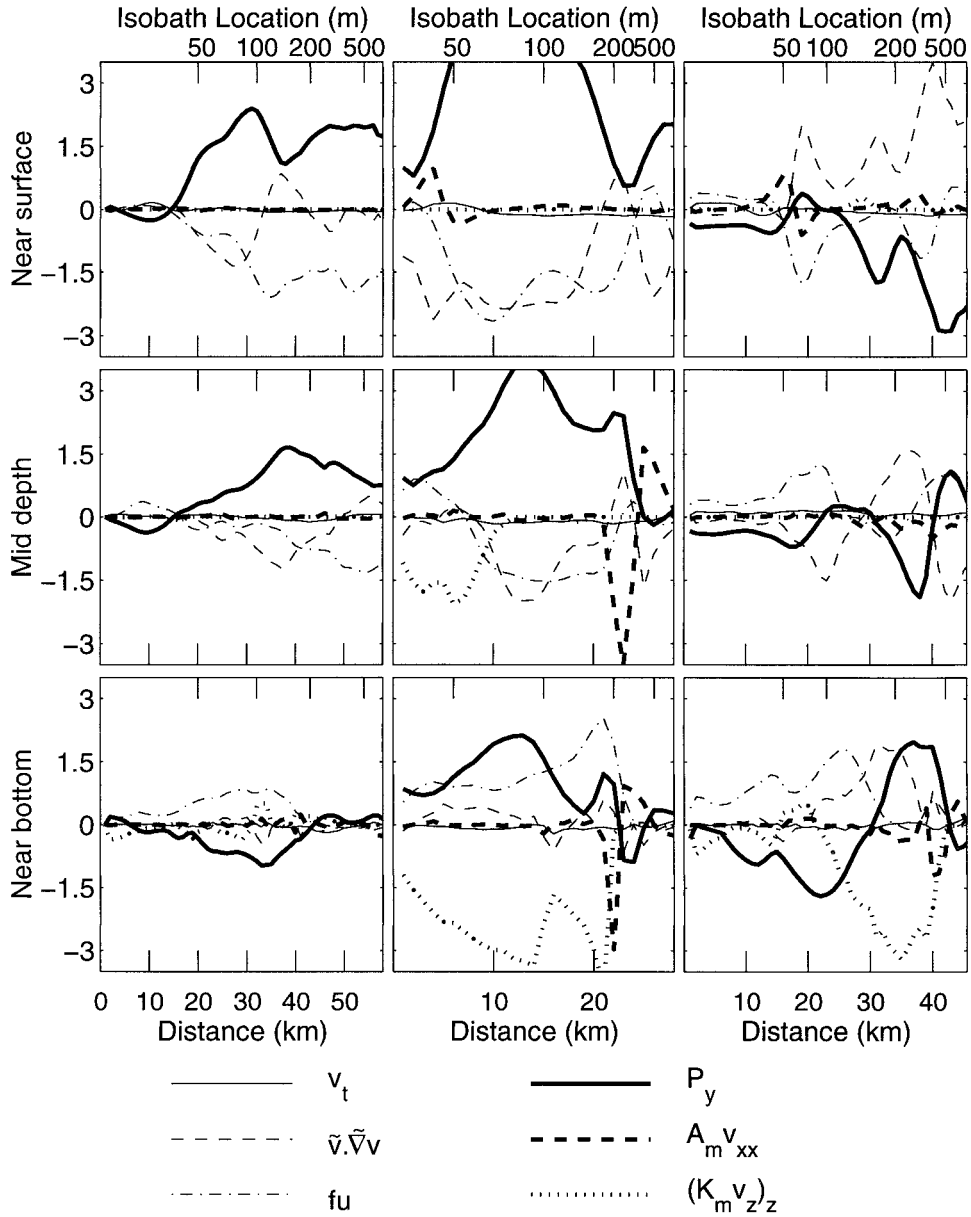

FIG. 12. Alongshelf momentum terms [(m s^{-1}) × 10^3] for zones 1, 2, and 3 (left to right) on day 15 from the EDM. The offshore distance and cross-shelf isobath locations are indicated at the bottom and top of each panel, respectively.

balance were P_y, fu and $\mathbf{v} \cdot \nabla v$, indicating that the flow was highly nonlinear, with advection due to the alongshelf flow being important and the dynamical balance tending toward geostrophy. In the NSZ in zones 2 and 3 the balances were much more complicated than in zone 1 with most of the terms becoming nonzero at some point.

Clearly the nonlinear, advective term $\mathbf{v} \cdot \nabla v$, was more dominant at zones 2 and 3, which is suggested to be an indicator of the three-dimensionality, or the alongshelf advective acceleration of the flow over the varying topography. The cross-shelf extent of the alongshelf acceleration can be inferred by this term, particularly at near-surface depths. This indicates that at zone 1 the alongshelf advective acceleration of the flow was unimportant. Conversely at zone 2, $\mathbf{v} \cdot \nabla v$ was dominant from the shelf break to the coast. This indicates that the EAC had a significant effect across the entire shelf including the NSZ. Below the regions where $\mathbf{v} \cdot \nabla v$ dominated, $(K_m v_z)_z$ was dominant in the BBL. At zone 3 the advective acceleration of the flow near the surface was limited to seaward of the 50-m isobath, which again corresponds well with the regions where $(K_m v_z)_z$ was dominant in the BBL. This correlation between the near-

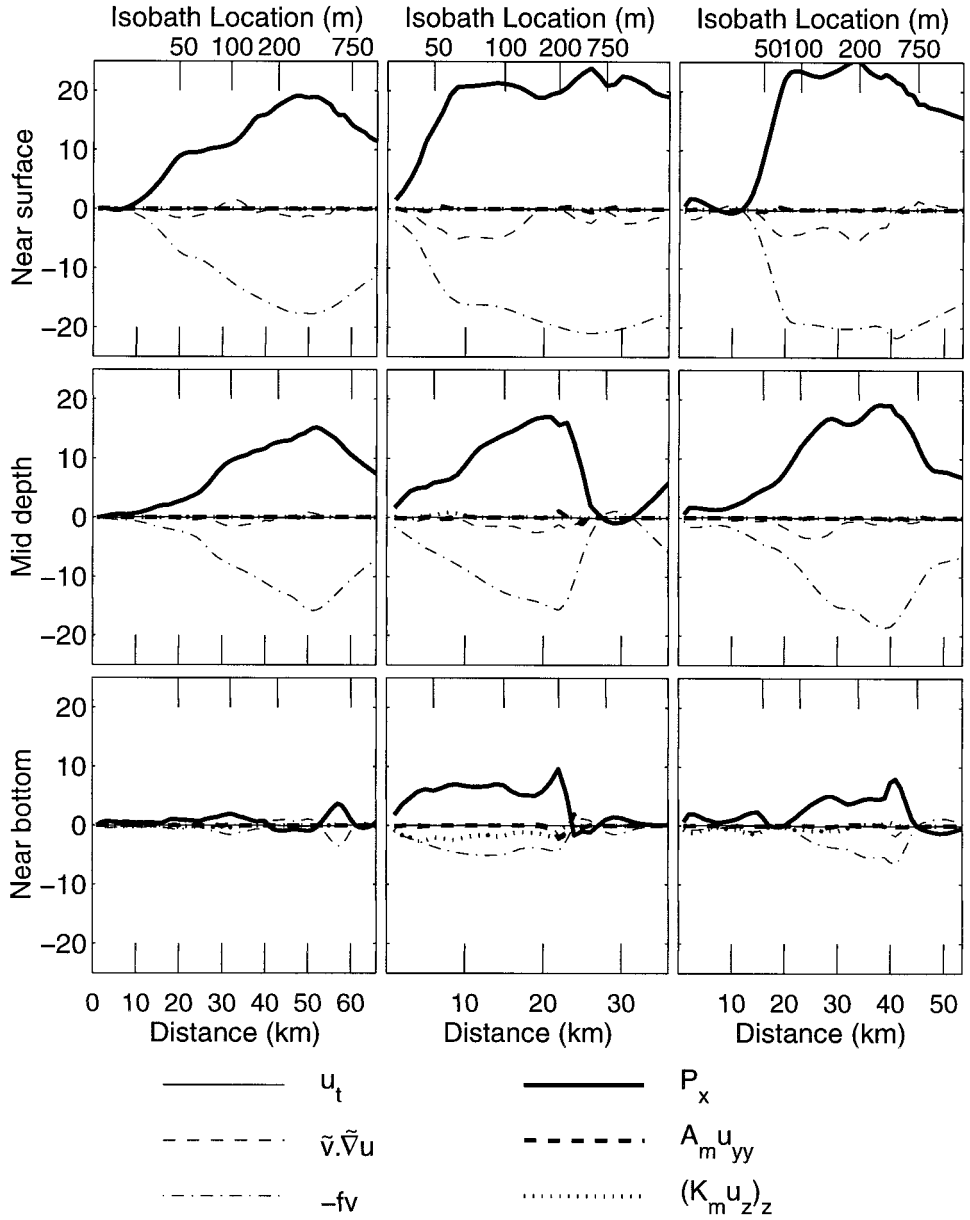

FIG. 13. Cross-shelf momentum terms [(m s^{-1}) × 10^3] for zones 1, 2, and 3 (left to right) on day 15 from the EDM. The offshore distance and cross-shelf isobath locations are indicated at the bottom and top of each panel, respectively.

surface advective acceleration and the high vertical diffusion in the BBL over the narrowing continental shelf adds weight to the argument that the accelerated EAC flow interfered with the geostrophic adjustment of the BBL flow, inhibiting BBL shutdown. The change in sign of $\mathbf{v} \cdot \nabla v$ between Cape Byron and Evans Head is perhaps an indication of a change in the rate of advective acceleration between the two zones.

The cross-shelf momentum balance in the interior and near the surface was unremarkable in all zones, with geostrophy clearly dominant. At some locations the advection term was nonzero; however the relative magnitude of this term was small compared the the geostrophic terms.

Recall that θ_t was positive in the BBL off Cape Byron over the mid shelf and negative over mid depths. This relationship is an indication of the mutual entrainment of the colder BBL water and the warmer interior water subject to the strong vertical mixing resulting from the EAC's interaction with the local topography.

This analysis was also performed for day 7.5, indicating the same qualitative balances. The magnitudes of the terms, particularly $(K_m v_z)_z$ and $(K_m u_z)_z$ in the BBL and $\mathbf{v} \cdot \nabla v$ and P_y in the mid and near-surface depths

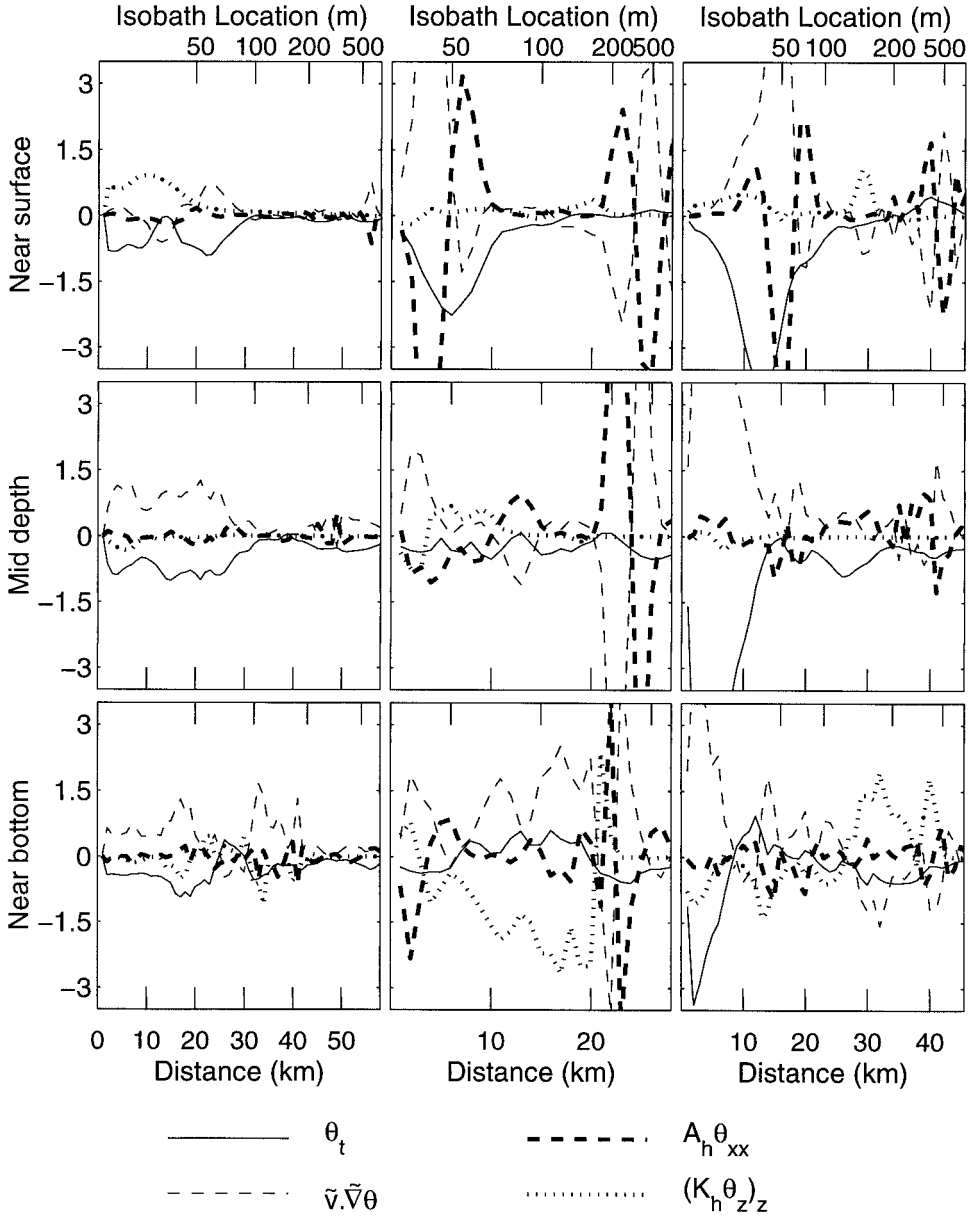

FIG. 14. Temperature equation terms (°C × 10^3) for zones 1, 2, and 3 (left to right) on day 15. The cross-shelf isobath locations are indicated on the top of each panel.

were about half those presented here for day 15. This temporal increase indicates that the balances discussed above were persistent and were not being attenuated through the BBL shutdown process of MacCready and Rhines (1993).

e. Analysis of the thermal wind relation

The finding that geostrophy was not ''exclusive'' in the BBL off Cape Byron has implications to the validity of the MacCready and Rhines (1993) BBL shutdown theory. As outlined in section 1, their theory assumes that the thermal wind relation, given in Eq. (1), is satisfied. In order to investigate this, the left-hand side (lhs) of the thermal wind relation $\partial v/\partial z$ and the right-hand side (rhs), $-[g/(f\rho_0)]\partial\rho/\partial x$, have been reconstructed in z coordinates from the sensitivity experiments 2–6, and is presented in Fig. 15. One would expect that the fields be equivalent, and indeed they are closely related; however the relation is clearly not satisfied for any of the experiments. The closest balance between the lhs and the rhs was in experiment 5, which had a decreased alongshelf transport. Recall that for this experiment, the BBL was not continuous from the shelf break to the coast, indicating that BBL shutdown was more dominant under these conditions.

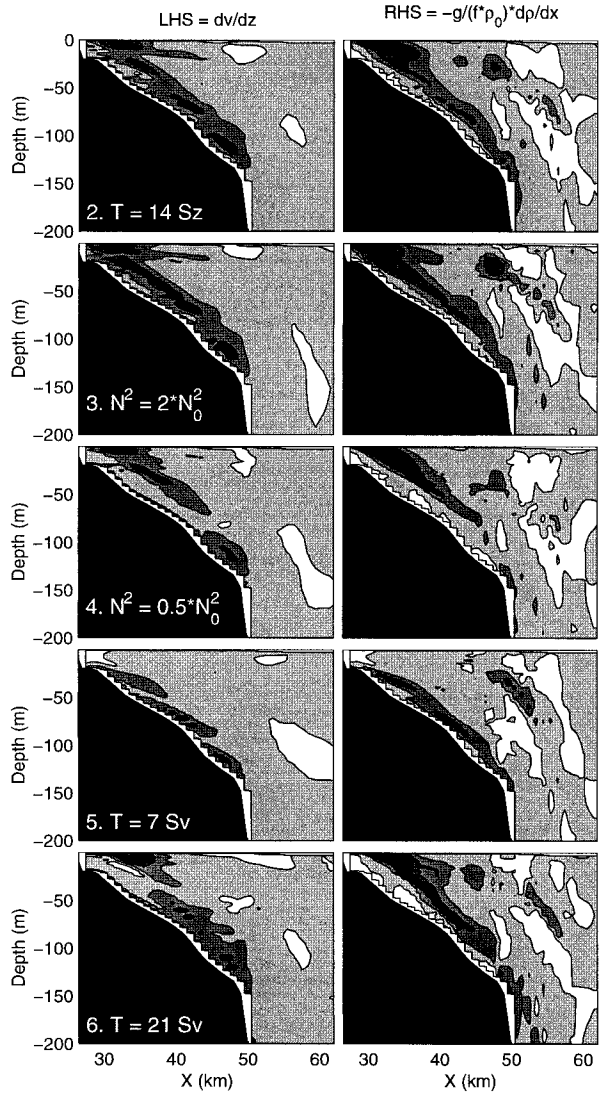

FIG. 15. Cross-sections off Cape Byron ($Y = 135$ km) of lhs (left) and rhs (right) of the terms in the thermal wind relation at day 15 for various sensitivity experiments described in Table 1. Contours range from -0.05 to 0 with an interval of 0.01.

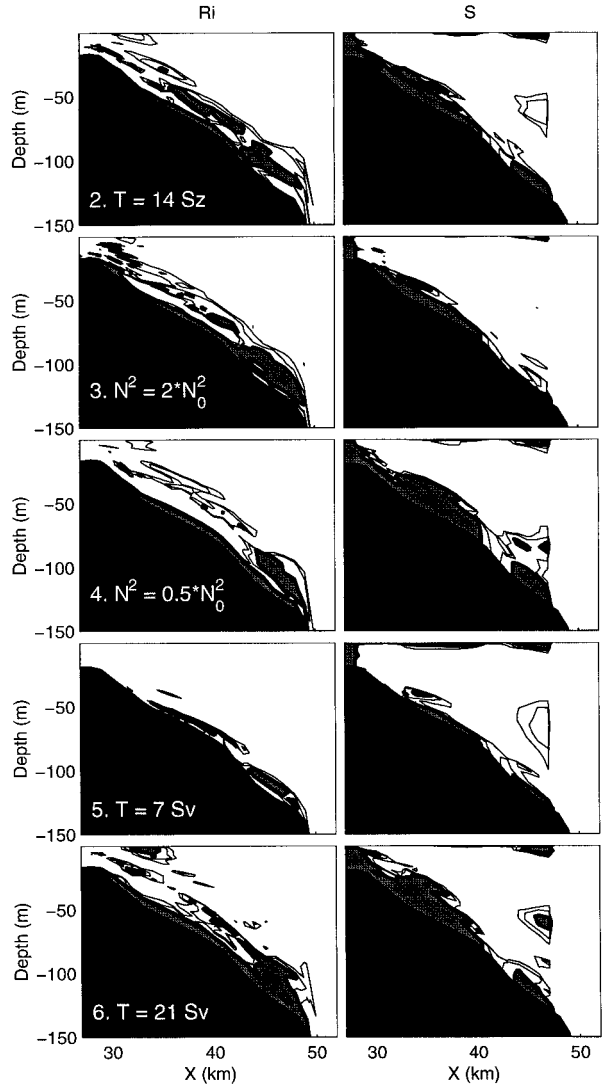

FIG. 16. As for Fig. 15 showing the local Richardson number (left) and the local Burger number (right). The gray, shaded region corresponds to areas where $\mathrm{Ri} < 0.2$ and $S < 0.2$, respectively. Contours range: $0 < \mathrm{Ri} < 1$ with intervals of 0.25 and $0 < S < 0.8$ with intervals of 0.2. Ri and S are greater than 1 in the interior.

Additional insight into why the thermal wind relation was not satisfied can be gained by considering the fields of the local Richardson number and the local Burger number, defined in Eqs. (2) and (3). These fields off Cape Byron on day 15 for experiments 2–6 are shown in Fig. 16. These fields show that within the BBL over much of the shelf the Richardson number was below, or close to, the critical value of 0.25. This characteristic of the flow explains why the vertical diffusion terms of the momentum and conservation equations were high in this region. For most of the experiments, the lowest Richardson number flow was located very close to the shelf break, which is beneath the strong, baroclinic EAC flow. This low Richardson number flow results in enhanced vertical mixing, which will be effective at mixing BBL and interior waters, as suggested in the analysis of the conservation equation for temperature. This characteristic has implications for the entrainment of nutrients into the EAC mean flow. Additionally the high vertical mixing in the BBL means that the local bouyancy frequency will be reduced, which in turn decreases the local Burger number, in Eq. (3). The fields of local Burger number indicate that a Burger number of below 0.2 was maintained in the BBL throughout the simulations, again with the exception experiment 5. As outlined in section 1 the low Burger number flow corresponds to an increased shutdown timescale of the BBL, explaining the persistence of the upwelling BBL flow. Beyond the shelf break, the near-bottom Burger number increases dramatically due to the increase in bottom

slope. For this reason the shutdown timescale is shorter off the shelf, which indicates that a logical ''upwelling limit'' of this type of current-driven upwelling is that upwelling waters originate no deeper than the shelf break.

5. Discussion

The baroclinic variables off Cape Byron showed the presence of a shoreward BBL flow on day 15. Consequently, the effect on the NSZ was to generate a thermal front, concentrated off Cape Byron, similar to that observed by OMb and Godfrey et al. (1980a).

A comparison of the magnitude and structure of the alongshelf velocity fields off Tweed Heads ($Y = 188$ km), Cape Byron ($Y = 135$ km), and Evans Head ($Y = 80$ km) in Fig. 17 shows that the EAC intensified near Cape Byron with strong currents in very close proximity to the shelf topography, confirming the suggestion that the EAC undergoes an advective, or Lagrangian, acceleration near Cape Byron. This feature explains the region of high bottom stress in this vicinity, indicating that the advective acceleration off Cape Byron increased near the bottom currents, consequently increasing the bottom stress. The region of high bottom stress off Evans Head was located offshore of the 175-m isobath. From Fig. 17 it is evident that at these depths the alongshelf velocities immediately above the bottom were nonzero; however shoreward of the 175 m isobath, the alongshelf velocities were very close to zero, explaining the isolation of the high bottom stress region. The reason for the current acceleration off Cape Byron can be un-

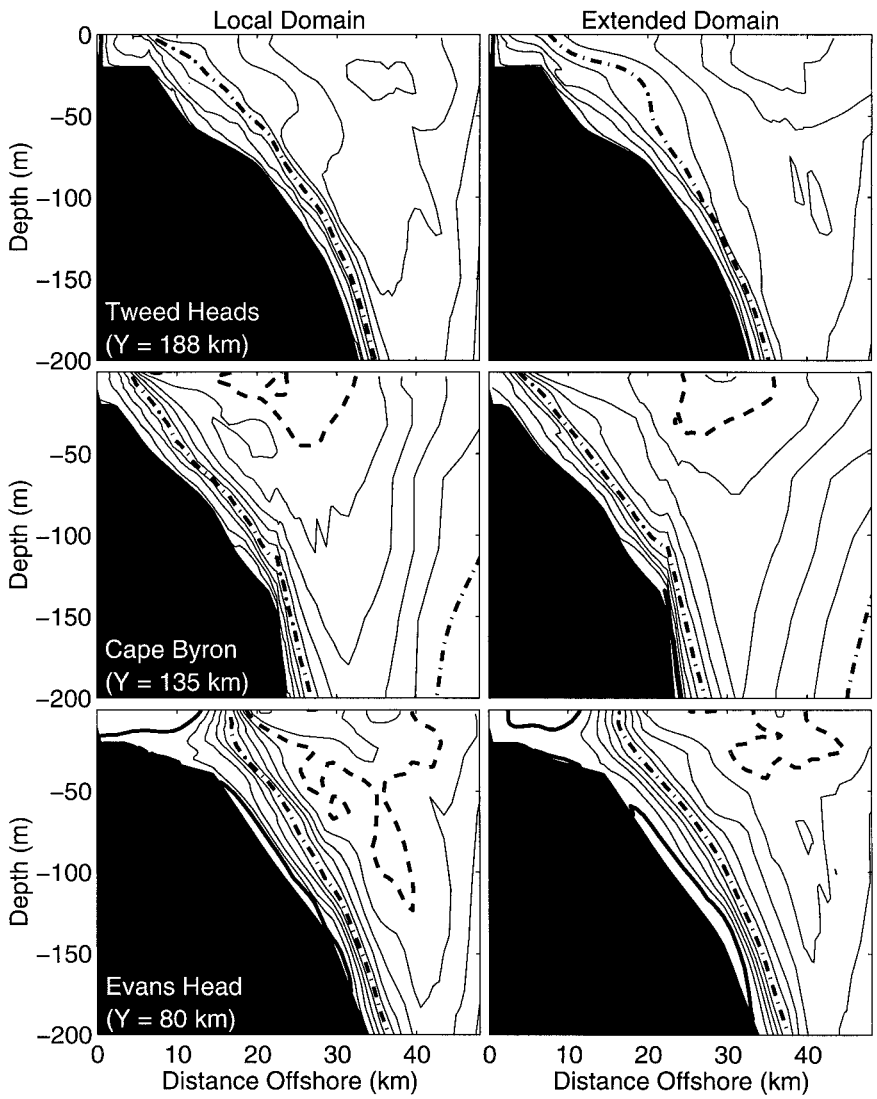

FIG. 17. Cross-sections of alongshelf velocity ($\Delta v = 0.1$ m s^{-1}) off Tweed Heads, Cape Byron, and Evans Head showing the -1.0 m s^{-1} (bold dashed), -0.5ms $^{-1}$ (bold dashed), and 0.0 m s^{-1} (bold solid) contours.

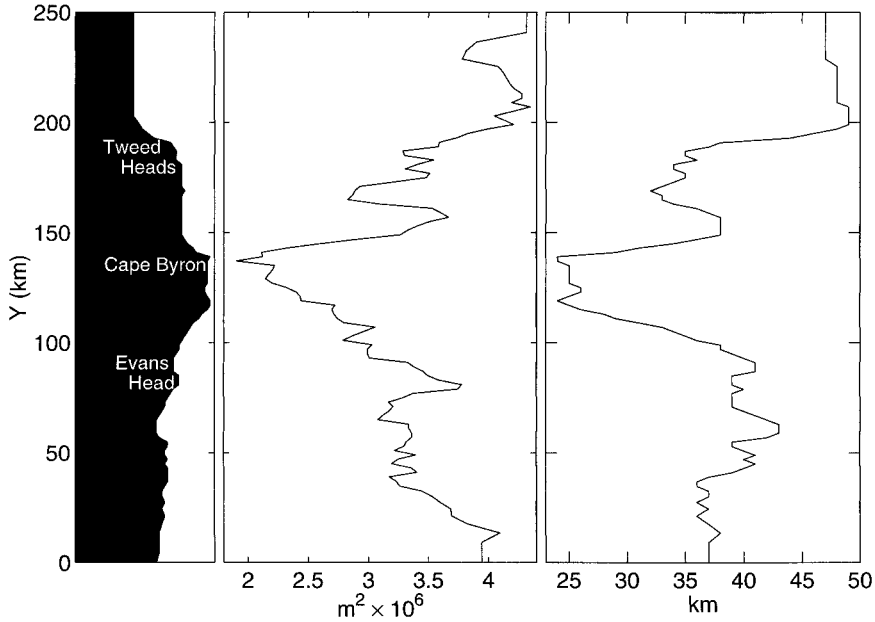

FIG. 18. Alongshelf variations of the cross-sectional area between the coast and the 300-m isobath (left) and the shelf width (right).

derstood by considering the alongshelf variations of the cross-sectional area of the shelf and the shelf width throughout the model domain (Fig. 18), which shows a minimum of both at Cape Byron. Consequently, it is proposed that, since the EAC is held to the continental slope by potential vorticity constraints, the flow is analogous to flow through a narrowing pipe. Such a flow exhibits its strongest flow at the narrowest point, which for the present study was Cape Byron. The strengthened currents acted to increase the near-bottom currents, resulting in an area of high bottom stress, which then drove the upwelling BBL, causing uplifting, and finally upwelling into the NSZ.

This upwelling mechanism, first identified by Hsueh and O'Brien (1971), is similar to that proposed by Boland (1979) and Blackburn and Cresswell (1993) for the EAC region; however neither have linked the topographic variation to the onset of upwelling. It is also consistent with the explanation posed by Rochford (1975) to explain upwellings off Laurieton, on the NSW central coast, which were unrelated to local winds. Blanton (1971) inferred a similar uplifting mechanism from observations in the Gulf Stream region; however it is unlikely that these intrusions were topographically induced since the alongshelf variation of the continental shelf width varies much more subtlely in the South Atlantic Bight. Observations presented by Gill and Schulmann (1979) off South Africa showed the acceleration of the alongshelf current over a gradually narrowing continental shelf, a feature similar to that modeled here.

As outlined in section 1, a strong argument against upwelling driven by an alongshelf flow has been presented by MacCready and Rhines (1993), who argued that subject to geostrophy, such a BBL would shutdown. It was shown in section 4 that the BBL flow was not purely geostrophic and that low Richardson number and low Burger number flow results in the persistence of an upwelling BBL flow. Furthermore, there was a definite correlation between the near-surface advection and the near-bottom vertical diffusion terms. The results from the conservation balance indicated that off Cape Byron the dominant balance in the BBL was

$$\mathbf{v} \cdot \nabla\theta = (K_h \theta_z)_z,$$

which further explains why BBL shutdown was not forthcoming. Since the strong vertical mixing between the cold upwelled waters and the warm interior waters acted to reduce the horizontal temperature (density) gradient between the upwelled BBL water and the interior, the vertical velocity shear that would normally act to reduce the bottom currents, by the thermal wind relation, was reduced, thus inhibiting the shutdown process. The Burger number in the BBL was very low on day 15, of the order of 0.15, which corresponds to a shutdown time of 7.5 days. If a constant upwelling BBL, with $u = 0.05$ ms^{-1}, was driven for 7.5 days, then the isotherm displacement is potentially of the order of 32.4 km, far in excess of the distance from the shelf break to the coast, which is around 21 km. These calculations indicate that, for the given Burger number, even a weak BBL flow driven by the EAC will be sufficient to establish a nearshore upwelled thermal front.

In a numerical study involving the configuration of a two-dimensional, cross-shelf model of the Sydney shelf, which assumed that the topography was homogeneous in the alongshelf direction, Gibbs et al. (1998)

argued that EAC-driven upwelling through a BBL was inefficient. They showed that such a BBL was shutdown within the first few days of simulation. Their results were validated by observations, justifying the assumption of homogeneous topography for the Sydney region. However, in this study it is suggested that the alongshelf topographic variations were crucial to the simulated upwelling and the results from the idealized cross-shelf model of Gibbs et al. (1998) are clearly not valid for this region.

The suggestion that the EAC does experience regions of high bottom stress along its path is further supported by the findings of Godfrey et al. (1980b), who used the distribution of different sediments along the east coast of Australia to infer the typical location of the EAC separation point. Godfrey et al. argued that where the coarsest sediment was located was an indication of where the EAC typically ''spins down,'' and separates from the coast. During this spindown, the sediment, which is entrained in the EAC flow, is deposited on the ocean floor. Of significance to this study is that such sediment is actively entrained in the EAC flow to the north of the separation point, indicating that a frictional interaction between the EAC and topography is a common occurrance.

6. Conclusions

The numerical experiments presented in this study indicate that alongshelf topographic variations can have a significant impact on the nearshore and shelf circulation. For the idealized scenario considered, involving the narrowing of the continental shelf near Cape Byron, it was clear that these variations accelerated the alongshelf flow through enhanced advection over mid and near-surface depths. As a result, the alongshelf, near-bottom currents were increased, resulting in an area of high bottom stress, which drove an upwelling BBL flow. This BBL flow was persistent throughout the simulations and was clearly not attenuated by BBL shutdown (MacCready and Rhines 1993) for most experiments. The analysis of the momentum equations indicated that an Ekman-like balance was dominant in the BBL and that the incidence of high vertical diffusion in the BBL was strongly related to high advection in the ocean interior. Furthermore, it is clear that the advective acceleration of the flow, along with the high level of vertical mixing between the upwelled BBL water and the interior shelf waters, interfered with the geostrophic adjustment of the BBL, resulting in a low Burger number flow with a correspondingly high shutdown timescale, thus explaining why BBL shutdown did not prevail. It was observed that the isotherm slopes quickly approached that of the bottom slope, at which point along-isopycnal mixing was maintained, without the opposing effects of buoyancy. This relationship provides a mechanism by which nutrient-rich slope waters are upwelled and entrained into the EAC mean flow. Such a mechanism has been sought in many observational studies of the EAC region (e.g., Tranter et al. 1986; Hallegraeff and Jeffrey 1993; Cresswell 1994) to explain how high levels of nutrients typically accompany EAC eddies commonly encountered along the NSW coast.

As a result of the persistent, topographically induced, EAC-driven upwelling a nearshore thermal front was generated in the NSZ, with similar characteristics to those observed by OMb and Godfrey et al. (1980a) off Cape Byron. Such fronts have been observed to have significant biological implications, representing regions of high productivity (e.g., Olsen et al. 1983). Since the nearshore fronts observed off eastern Australia are generated by EAC-driven upwelling, they are likely to be seasonal and dependent on the strength of the EAC. This seasonal dependence is supported by the common repeated observations of an upwelled, thermal front in the vicinity of Cape Byron in spring and summer periods. This dependence was verified by a sensitivity test in section 3, where it was shown that a decrease (increase) in the magnitude of the alongshelf transport, corresponded to a weakening (strengthening) of the shoreward BBL flow, consequently reducing (increasing) the amount of cold water upwelled to the surface.

In addition to this mechanism being identified, a comparison between a LDM and a larger EDM were made. Although the results from both model configurations were in good agreement, it was clear that there are significant advantages in extending the model domain, with homogeneous topography, where lateral boundary forcing is imposed. This allows the model physics to adjust the internal structure of the baroclinic variables before the realistic topographic influences are encountered by the flow.

Acknowledgments. This work was supported by the Australian Research Council through grants to Jason Middleton and by an Australian Postgraduate Research Award to Peter Oke. The Australian National University is also acknowledged for making available the Fujitsu VPP300 Supercomputer for this research. The support of the Australian National Greenhouse Advisary Committee is also acknowledged.

REFERENCES

Allen, J. S., P. A. Newberger, and J. Federiuk, 1995: Upwelling circulation on the Oregon continental shelf. Part I: Response to idealized forcing. *J. Phys. Oceanogr.,* **25,** 1843–1866.

Beckman, A., and D. B. Haidvogel, 1993: Numerical simulation of flow around a tall seamount. Part I: Problem formulation and model accuracy. *J. Phys. Oceanogr.,* **23,** 1736–1753.

Blackburn, S. I., and G. R. Cresswell, 1993: A coccolithophorid bloom in Jervis Bay, Australia. *Aust. J. Mar. Freshwater Res.,* **44,** 253–260.

Blanton, J., 1971: Exchange of Gulf Stream Water with North Carolina shelf water in Onslow Bay during stratified conditions. *Deep-Sea Res.,* **18,** 167–178.

Blumberg, A. F., and G. L. Mellor, 1983: Diagnostic and prognostic

numerical circulation studies of the South Atlantic Bight. *J. Geophys. Res.,* **88,** 4579–4592.

——, and L. H. Kantha, 1985: Open boundary conditions for circulation models. *J. Hydr. Eng.,* **111,** 237–255.

——, and G. L. Mellor, 1987: A description of a three-dimensional coastal ocean circulation model. *Three-Dimensional Coastal Ocean Models,* Vol. 4, N. Heaps, Ed., Amer. Geophys. Union, 1–16.

Boland, F. M., 1979: A time series of expendable bathythermograph sections across the East Australian Current. *Aust. J. Mar. Freshwater Res.,* **30,** 303–313.

Boucher, J., F. Ibanez, and L. Prieur, 1987: Daily and seasonal variations in the spatial distribution of zooplankton populations in relation to the physical structure in the Ligurian Sea Front. *J. Mar. Res.,* **45,** 133–173.

Church, J. A., and G. R. Cresswell, 1986: Oceanographic features of Southeast Australian Waters. CSIRO Marine Laboratories Internal Summary Rep. [Available from CSIRO Marine Research, GPO Box 1538, Hobart, Tasmania 7001, Australia.]

Cresswell, G. R., 1994: Nutrient enrichment of the Sydney continental shelf. *Aust. J. Mar. Freshwater Res.,* **45,** 677–691.

——, C. Ellyett, R. Legeckis, A. F. Pearce, and R. Boyd, 1983: Nearshore features of the East Australian Current system. *Aust. J. Mar. Freshwater Res.,* **34,** 105–114.

Flather, R. A., 1976: A tidal model of the northwest European continental shelf. *Mem. Soc. Roy. Sci. Leige, Ser. 6,* **10,** 141–164.

Garret, C., P. MacCready, and P. Rhines, 1993: Boundary mixing and arrested Ekman layers: Rotating stratified flow near a sloping boundary. *Annu. Rev. Fluid Mech.,* **25,** 291–323.

Gibbs, M. T., J. H. Middleton, and P. Marchesiello, 1998: Baroclinic response of Sydney shelf waters to local wind and deep ocean forcing. *J. Phys. Oceanogr.,* **28,** 178–190.

Gill, A. E., and E. H. Schulmann, 1979: Topographically induced changes in the structure of an inertial coastal jet: Application to the Agulhas Current. *J. Phys. Oceanogr.,* **9,** 975–991.

Godfrey, J. S., G. R. Cresswell, and F. M. Boland, 1980a: Observations of low Richardson numbers and undercurrents near a front in the East Australian Current. *J. Appl. Meteor.,* **10,** 301–307.

——, ——, T. J. Golding, and A. F. Pearce, 1980b: The separation of the East Australian Current. *J. Phys. Oceanogr.,* **10,** 430–440.

Hallegraeff, G. M., and S. W. Jeffrey, 1993: Annually recurrent diatom blooms in spring along the New South Wales coast of Australia. *Aust. J. Mar. Freshwater Res.,* **44,** 325–334.

Hitchcock, G. L., A. J. Mariano, and T. Rossby, 1993: Mesoscale pigment fields in the Gulf Stream: Observations in a meander crest and trough. *J. Geophys. Res.,* **98,** 8425–8445.

Hsueh, Y., and J. J. O'Brien, 1971: Steady coastal upwelling induced by an along-shore current. *J. Phys. Oceanogr.,* **1,** 180–186.

Hynd, J. S., 1969: Isotherm maps for tuna fisherman. *Aust. Fish.,* **28**(7), 13–22.

Levitus, S., 1982: *Climatological Atlas of the World Ocean.* NOAA Prof. Paper No. 13, U.S. Department of Commerce, National Oceanographic and Atmospheric Administration, 173 pp.

MacCready, P., and P. B. Rhines, 1993: Slippery bottom boundary layers on a slope. *J. Phys. Oceanogr.,* **23,** 5–22.

Mahadevan, A., J. Oliger, and R. Street, 1996: A nonhydrostatic mesoscale ocean model. Part I: Well-posedness and scaling. *J. Phys. Oceanogr.,* **26,** 1868–1880.

Mellor, G. L., and T. Yamada, 1982: Development of a turbulence closure model for geophysical fluid problems. *Rev. Geophys. Space Phys.,* **20,** 851–875.

——, T. Ezer, and L.-Y. Oey, 1994: The pressure gradient conundrum of sigma coordinate ocean models. *J. Atmos. Oceanic Technol.,* **11,** 1126–1134.

NOAA, 1988: NGDC data announcement 88-MG-02: Digital relief of the surface of the Earth. U.S. Department of Commerce, NOAA, NGDC, Boulder, CO.

Oke, P. R. and J. H. Middleton, 2000: Nutrient enrichment off Port Stephens: the Role of the East Australian Current. *Contin. Shelf Res.,* in press.

Olsen, D. B., O. B. Brown, and S. R. Emmerson, 1983: Gulf Stream frontal statistics from Florida Straits to Cape Hatteras derived from satellite and historical data. *J. Geophys. Res.,* **88,** 4569–4577.

Palma, E. D., and R. P. Matano, 1998: On the implementation of passive open boundary conditions for the Princeton Ocean Model: The barotropic mode. *J. Geophys. Res.,* **103,** 1319–1341.

Ridgway, K. R., and J. S. Godfrey, 1997: Seasonal cycle of the East Australian Current. *J. Geophys. Res.,* **102,** 22 921–22 936.

Rochford, D. J., 1972: Nutrient enrichment of East Australian coastal waters. I. Evans Head upwelling. CSIRO Aust. Div. Fish. Oceanogr. Tech. Paper 33, 1-37. [Available from CSIRO Marine Research, GPO Box 1538, Hobart, Tasmania 7001, Australia.]

——, 1975: Nutrient enrichment of East Australian coastal waters. II. Laurieton upwelling. *Aust. J. Mar. Freshwater Res.,* **26,** 233–243.

Smagorinsky, J., 1963: General circulation experiments with primitive equations, I. The basic experiment. *Mon. Wea. Rev.,* **91,** 99–164.

Stanton, B. R., 1976: An oceanic frontal jet near the Norfolk Ridge north-west of New Zealand. *Deep-Sea Res.,* **23,** 821–829.

Tranter, D. J., D. J. Carpenter, and G. S Leech, 1986: The coastal enrichment effects of the East Australian Current eddy field. *Deep-Sea Res.,* **33,** 1705–1728.